

Article

Integrated Waste-to-Energy Process Optimization for Municipal Solid Waste

Hossam A. Gabbar *  and Muhammad Sajjad Ahmad

Department of Energy and Nuclear Engineering, Faculty of Engineering and Applied Science, Ontario Tech University (UOIT), Oshawa, ON L1H 7K4, Canada; muhammad.ahmad@ontariotechu.ca

* Correspondence: hossam.gaber@ontariotechu.ca

Abstract: Within the past few decades, thousands of experiments have been performed to characterize urban waste and biomass to estimate their bioenergy potential and product identification. There is a need to develop an integrated process model based on the experimental literature, as well as simulations to obtain suitable products. In this study, municipal solid waste (MSW), including paper and plastic characterization and an integrated process model, were developed to optimize the final products in a reactor system. The process model has two modes, R&D and reactor control (RC), to obtain suitable products including bio-oil, char, and gases. A database was integrated based on thermokinetics, machine learning, and simulation models to optimize product efficiency. The experimental data include those obtained by thermogravimetric analysis and Fourier-transform infrared spectroscopy, which were linked to a pyrolysis experimental setup. Feedstock product mapping models were incorporated into the database along with the temperature, heating rates, elemental analysis, and final product concentration, which were utilized for the pyrolysis reactor setup. Product feasibility was conducted based on life cycle cost, affordability, and product efficiency. The present work will bridge the gap between experimental studies and decision-making based on obtained products under several experimental conditions around the world.

Keywords: process optimization; waste conversion; life cycle analysis; machine learning



Citation: A. Gabbar, H.; Ahmad, M.S. Integrated Waste-to-Energy Process Optimization for Municipal Solid Waste. *Energies* **2024**, *17*, 497. <https://doi.org/10.3390/en17020497>

Academic Editor: Massimo Dentice D'Accadia

Received: 1 December 2023

Revised: 14 January 2024

Accepted: 17 January 2024

Published: 19 January 2024



Copyright: © 2024 by the authors. Licensee MDPI, Basel, Switzerland. This article is an open access article distributed under the terms and conditions of the Creative Commons Attribution (CC BY) license (<https://creativecommons.org/licenses/by/4.0/>).

1. Introduction

In recent decades, the focus of energy generation has diverted from fossil fuels to renewable energy resources. Sustainable waste conversion into renewable energy gained significant momentum due to the initiative from the European Green Deal (EGD) [1,2]. The European Green Deal is a key policy initiative toward the sustainable goal aims of transforming the EU into a resource-efficient and competitive economy, achieving net-zero greenhouse gas emissions by 2050, which is also a priority of the Canadian government. The ambitious strategy shared by both continents plays a pivotal role in our current research, which concentrates on key factors such as providing affordable energy, creating a fully integrated system for minimizing waste by converting it into valuable products, and enhancing energy efficiency by exploring new possibilities in renewable energy sources, as indicated in industry references [1,2]. Various initiatives under the European Green Deal (EGD), like the transition to clean energy through renewable energy resources and reducing emissions, are underway. These efforts align with the Canadian government's goals to cut down emissions and optimize integrated solutions. The overarching objective is to establish a comprehensive system for effectively managing waste streams to produce beneficial products and chemicals.

Municipal solid waste (MSW) management is a crucial component in the advancement of the bioeconomy, as it is considered the primary source for bioenergy generation in the United States, Canada, and Brazil [3]. However, the utilization of biomass presents a challenge due to the diverse range of feedstocks and complex chemical structures [4].

Global plastic consumption was estimated to be 299 million tons in 2013, with an expected increase by several folds by 2050, which is alarming to the earth due to its difficulty in degrading in the environment and rapidly trailing landfills [5,6]. Process optimization plays a critical role in converting raw materials like paper waste and plastic waste (PPW) into valuable products and chemicals through experiments and computational work [7]. Currently, there are only a limited number of innovative process integration models that have emerged in the United States, Brazil, and certain regions of Europe, and further investigation into their development is necessary [8,9]. Nonetheless, a significant amount of research is being conducted on low-carbon and carbon-neutral technologies [10]. A wide range of waste-to-energy conversion technologies are available, including gasification, anaerobic digestion, coal-fired boilers, power plants, and biomass-to-ethanol processes (as well as other methods for producing transportation fuels) [11]. Pressurized anaerobic digestion through autogenerative high pressure [12], pressurized anaerobic digestion [13], and two-stage digestion [14] has improved the conversion of methane content into biogas. In another study, a reliability model using diesel engines while operating on biofuel was proposed [15]. Therefore, it is reasonable to inquire about the optimal combination of technologies, biomass types, and their locations that would result in the most efficient (i.e., cost-effective) approach to the expansion of the MSW industry both domestically and internationally. This work aims to formulate an optimization strategy to address these questions.

The process of thermochemical conversion of plastic and waste involves the utilization of a distributed network of fast pyrolyzers to thermally transform biomass into synthesis gas (syngas), bio-oil, and biochar [16]. This approach presents a sustainable means of generating energy from plastics and paper waste, as the syngas produced can provide the energy needed for the pyrolysis process. The resulting bio-oil is a valuable energy source, with a calorific value of approximately 17 MJ/kg, which can be used for heat generation or sent to a refinery for further processing into transportation fuels [17]. Biochar produced from the co-pyrolysis of plastic and wastes can improve soil quality in many ways. However, it is challenging to define the exact thermochemical conditions required, due to the complex nature and structure of biomass, to obtain different products (biofuel, gases, biochar) [18]. The co-pyrolysis process of PPW including corn straw, corn stover, and barley straw and plastic waste needs to be optimized, which will help in improving product recovery and energy efficiency alongside machine learning processes.

In the past few decades, numerous studies have focused on optimizing thermochemical processes (pyrolysis, gasification) to produce valuable products (biofuel, biogas, and biochar). A few have focused on utilizing biosolids from large industrial and municipal solid waste plants to detoxify the residuals and produce biochar and/or bio-oil simultaneously. In addition, minimal research has been conducted on the co-pyrolysis of biomass and plastic. A recent study showed that the biochar yield improved by 44–49% by using the co-pyrolysis of biomass and plastic instead of single pyrolysis [19]. However, the synergetic effects of char yield lower the pyrolysis temperature when mixing biomass with different ratios (25–50%) of plastic derivatives [20]. Another study focused on achieving different favorable optimizations of development temperature ranges for the co-pyrolysis of plastic and tires. But more critical aspects of co-pyrolysis were not explored including the underlying mechanism, thermokinetics, and synergetic effects of developing improved mechanistic models to obtain co-pyrolysis products [21]. Likewise, a co-pyrolysis study on truck tires and fruit bunches increased oil yield by 20% as compared to single tire pyrolysis [22]. Furthermore, a recent study quantified pyrolytic and gaseous products through machine learning approaches [23]. Therefore, using machine learning in the co-pyrolysis process of paper and plastic MSW is a novel idea in integrated biorefinery. Therefore, an optimization framework for the strategic identification, development and commercialization of bio-based feed stocks for biomaterials, biochemicals, and bioenergy will first be developed. The model will seek to provide an understanding of emerging opportunities and their underlying challenges for solid waste management companies, and the applicability of

the model will be demonstrated with a case study focusing on new markets for MSW's operations. An integrated analytical framework will also be applied to comparing the results with the recent literature [24]. However, several barriers [25] to the integration of the process model must first be identified including by using recommendations provided to develop integrated process models in other parts of Canada by policy makers wishing to facilitate the development of novel biomass or other paper waste in other parts of Canada.

The current study presents an exploratory case study analysis of paper waste and plastic MSW through process integration to develop biobased production systems. MSW was selected due to its abundance and easy availability, whereas plastic derivatives are hard to degrade and combustion is an environmental harm. Therefore, it would be important to know the co-pyrolysis behavior of MSW, wherever paper waste is a profuse biological resource while plastic is a detrimental environmental waste. Considering Canada's abundant natural resources, the utilization of lignocellulosic residues obtained from agricultural sources and plastic derivatives as feedstocks presents a favorable opportunity for the development of advanced biofuel and biochar utilization industries [26]. Therefore, it would be worthwhile to produce valuable chemicals and products from an MSW-handling industry. In the upcoming years, with the growing population of Ontario, it will be crucial to address the proper conversion of these waste materials into useful chemicals and products [27]. The economic feasibility of biobased materials relies on the optimization of their efficiency and the reduction in toxic gas emissions during pyrolysis, gasification, and combustion processes.

A complete range of experimental and simulation analyses were performed including process system engineering, reaction engineering, pyrolysis, and co-pyrolysis experiments to obtain useful energy products (bio-oil, gases, biochar) in terms of energy generation and product optimization. Therefore, each pyrolysis product (bio-oil, gases, biochar) recovery will also be optimized through some complex mechanistic models through machine learning and detailed experimental characterization [28]. As a result, it is possible to provide the cheapest solution for the industrialist to adopt our expanded new strategy to contrivance in large-scale reactor modeling. It will also help to determine the overall cost of the process, including the rate at which the MSW is bought, and the financial and environmental benefits. We will also address the loopholes to finalizing this co-pyrolysis technology.

The integrated process includes a series of experiments linked with simulations and mathematical models to obtain optimized products and chemicals. The process has four major stages linked with each other throughout the process integration. It started with the characterization of a raw MSW sample and performance of thermogravimetric analyses to obtain different patterns and temperature profiles with heating rates and specific temperature ranges. The products were identified based on their temperature regions and kinetic parameters were identified to be used in the second stage, the simulation process. In the second stage, simulation through Aspen Plus was performed by inputting temperature profiles and kinetic parameters to obtain products. In the third stage, elemental analysis data were used that were generated through experiments and the literature to fit with the final products. Moreover, a life cycle cost analysis was performed to obtain the cost and benefit analyses of the major products. The novelty of this work resides in the amalgamation of experiments performed compared to recent decades of characterization of waste. No such effort was made for each process that was linked with one another through control systems to obtain useful products by changing input parameters such as temperature ranges, heating rates, and process conditions. It was only possible when an integrated system was introduced by incorporating experimental data and using this data to build experimental strategies to obtain optimized products. This strategy may reduce the cost, chemical usage, and time required to target the desired products.

2. Materials and Methods

A series of experiments were conducted in triplicate including thermogravimetric analysis, machine learning, pyrolysis, and simulation modeling as shown by the detailed

framework in Figure 1. The various ranges of parameters were investigated during each stage including thermal degradation patterns, kinetic and thermodynamic parameters, elemental contents, reaction conditions, gaseous products, and life cycle costs.

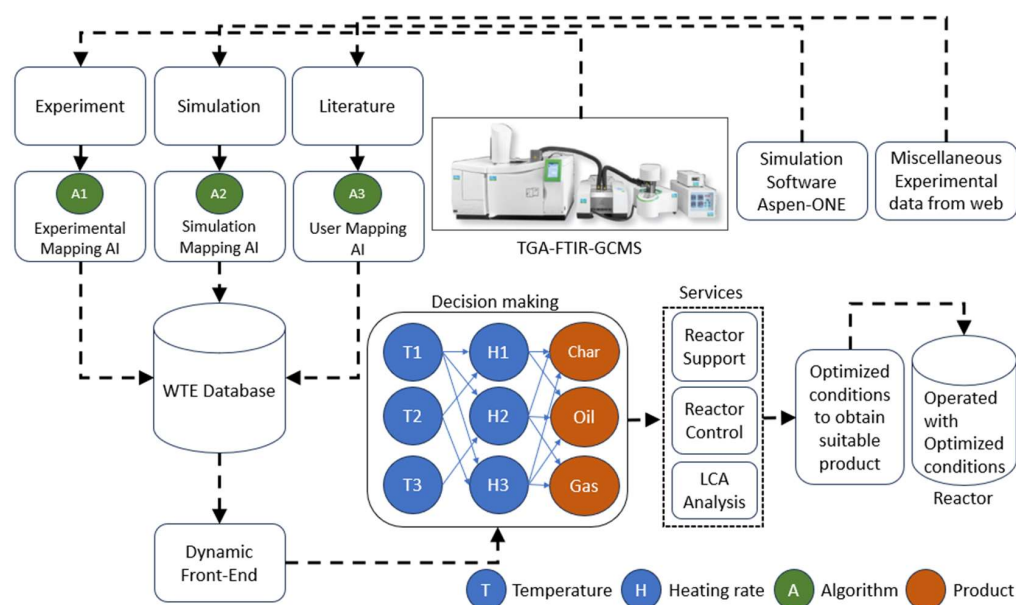


Figure 1. Integrated framework to optimize pyrolysis products.

2.1. Integration of the Experimental Setup (Reactor) with a TG-FTIR-GCMS System

The experimental setup was connected, including a TGA-FTIR and GCMS, to characterize the small amount of the MSW to obtain products and to study their reaction chemistry. For this purpose, a 10 mg sample was characterized in a controlled nitrogen environment at different heating rates (10–40 °C/min) to study its reaction chemistry. A kinetic analysis was also performed using different isoconversion models to obtain thermogravimetric parameters including the activation energy, pre-exponential factor, enthalpy, entropy, and Gibbs' free energy. These parameters were stored in a database for future reference and to obtain suitable products based on experimental conditions. The obtained analysis results were stored in a database integrated as a part of process model to analyze the feasibility of the products through a laboratory-scale pyrolysis process. The integrated algorithm to obtain the thermodynamic and reaction chemistry is shown in Figure 2. Interventionary studies involving animals or humans, and other studies that require ethical approval, must list the authority that provided approval and the corresponding ethical approval code.

The evaluation of the reaction mechanism underlying biomass degradation is difficult due to the complexity of the chemical makeup of biomass. Kinetic analysis is a useful tool for assessing the thermal stability of materials during combustion and pyrolysis. A single-step biomass degradation process is shown in Equation (1) as the following:



The instantaneous conversion function α and the pyrolytic temperature have an impact on the rate of the chemical reaction. Consequently, it can be expressed as follows in Equation (2):

$$\alpha = \frac{m_0 - m_t}{m_0 - m_\infty} \quad (2)$$

where m_0 denotes the initial mass, m_t denotes its mass at a certain point in the reaction time (t), and m_∞ denotes its mass at the end of the reaction.

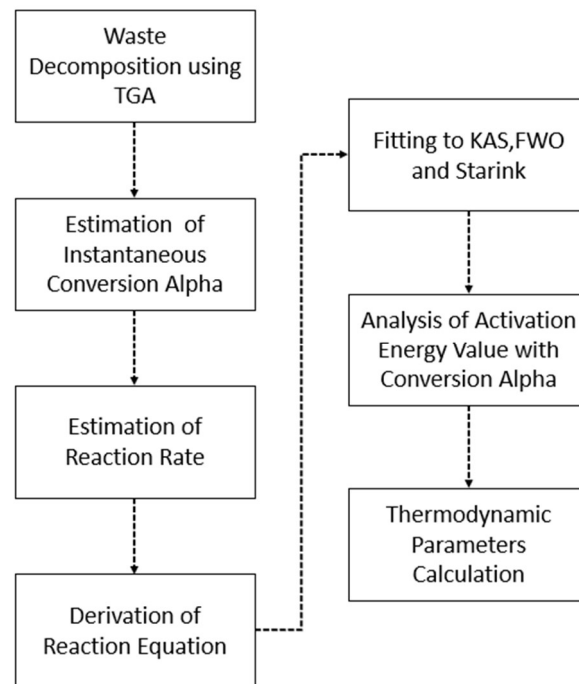


Figure 2. Integrated algorithm to obtain thermodynamic and reaction chemistry parameters.

The response rate, $d\alpha/dt$, which is a function of α in these processes, can be expressed as follows in Equation (3):

$$\frac{d\alpha}{dt} = kf(\alpha) \quad (3)$$

where Equation (3) is the fundamental kinetic equation for solid-state mass loss processes. In the case of thermally stimulated processes, the Arrhenius equation is frequently used to replace the value of the rate constant k , like in Equation (3), which then has the following form:

$$\frac{d\alpha}{dt} = A \exp\left(\frac{-E_\alpha}{RT}\right) f(\alpha) \quad (4)$$

where A is the pre-exponential factor, E_α is the energy of activation, $f(\alpha)$ is the function of the degree of conversion, called the reaction model, and R is the gas constant. In terms of physics, A describes the frequency of collisions between the particles involved in the production of activated complex(es), E_α is the activation energy barrier(s), and $f(\alpha)$ is an expression for the reaction mechanism.

Re-arranging Equation (3) gives

$$\frac{d\alpha}{f(\alpha)} = A \exp\left(\frac{-E_\alpha}{RT}\right) dt \quad (5)$$

Substituting the constant heating rate (with increasing temperature),

$\beta = \frac{dT}{dt} = \frac{dT}{d\alpha} \times \frac{d\alpha}{dt}$, in Equation (5) gives

$$g(\alpha) = \int_0^\alpha \frac{d\alpha}{f(\alpha)} = \frac{A}{\beta} \int_0^T \exp\left(\frac{-E_\alpha}{RT}\right) dT \quad (6)$$

The term $g(\alpha)$ is the integral expression of the conversion-dependent function, while the term used in Equation (6) is the integral of the temperature, which lacks an explicit integral solution. After resolving numerous empirical interpolation equations, several researchers have put forth an approximation of the solution.

Calculations of the KAS, OFW, and Starink methods can be established as the following:

$$\ln \beta_i = \ln \left(\frac{A_\alpha E_\alpha}{Rf(\alpha)} \right) - 5.331 - 1.052 \frac{E_\alpha}{RT_{\alpha,i}} = \text{constant} - 1.052 \frac{E_\alpha}{RT_{\alpha,i}} \quad (\text{OFW}) \quad (7)$$

$$\ln \left(\frac{\beta}{T^2} \right) = \ln \left(\frac{AR}{E_\alpha g(\alpha)} \right) - \frac{E_\alpha}{RT} \quad (\text{KAS}) \quad (8)$$

$$\ln \left(\frac{\beta}{T^{1.92}} \right) = \ln \left(\frac{AR}{E_\alpha g(\alpha)} \right) - \frac{E_\alpha}{RT} \quad (\text{Starink}) \quad (9)$$

The thermodynamic parameters in this study, including ΔG , ΔH , and ΔS , were determined using the following formulas:

$$\Delta H = E - RT \quad (10)$$

$$\Delta G = E + RT_p \ln \left(\frac{k_B T_p}{hA} \right) \quad (11)$$

where k_B is the Boltzmann constant, which has a value of $1.38 \times 10^{-23} \text{ J K}^{-1}$.

$$\Delta S = \frac{\Delta H - \Delta G}{T_p} \quad (12)$$

2.2. Simulation Integration in the Process Model with Machine Learning

The simulation software results were integrated to obtain suitable products and analysis based on the simulation results related to the temperature and heating rate conditions. The simulation was used to obtain the gaseous products based on the elemental analysis results which also integrated with the process model. Using the ASPEN Plus process simulator, a stoichiometric steady-state model was created in order to mimic the process of municipal solid waste. The elemental analysis results of five samples, MSW1, MSW2, MSW3, MSW4, and MSW5, were used as inputs to be simulated based on our previous studied data [29]. The model was used to study the influence of proximate and ultimate analysis on gasification behavior. Additionally, it was utilized to break down volatile yields that were produced during the process.

On the other hand, machine learning algorithms were used to map the elemental results to obtain suitable pyrolysis products. The major equations used are described below and the algorithm is shown in Figure 3.

Equations for Machine Learning

The following equations were used to calculate the residual sum of squares, meaning the error between the predicted and modeled values; the hyperbolic tangent function, representing the activation function in our model; the logistic sigmoid function, which is a non-linear function that allows neural networks to learn and represents complex patterns; and the Gaussian function, representing the initial weights of random values and used to perform regression and classification tasks.

$$SSE = 1/2N \sum_{i=1}^n (y_i - t_i) \quad (13)$$

$$\text{Hyperbolic Tangent} = \frac{e^a + e^{-a}}{e^a + e^{-a}} \quad (14)$$

$$\text{Logistic Sigmoid} = \frac{1}{1 + e^{-a}} \quad (15)$$

$$\text{Sin} = \text{Sin}(\alpha) \quad (16)$$

$$\text{Gaussian} = \frac{1}{2\pi\sigma} e^{-\frac{(x-u)^2}{2\sigma^2}} \quad (17)$$

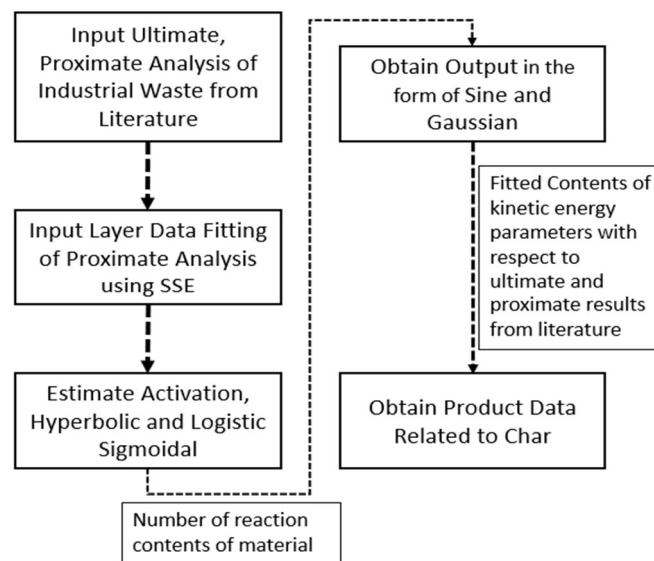


Figure 3. Integrated algorithm to obtain pyrolysis products.

2.3. Process Model Integrated with a WTE Database

To further power the process model designs, a database was integrated in the laboratory-scale reactor. It was integrated with datasets obtained from the experimental, simulation, and literature data related to the temperature profiles, mass degradation patterns, heating rates, and product analyses of similar waste samples. It gave information regarding mass degradation patterns at different heating rates and temperature ranges which could further be validated through our experimental setup values, as shown in Figure 4.

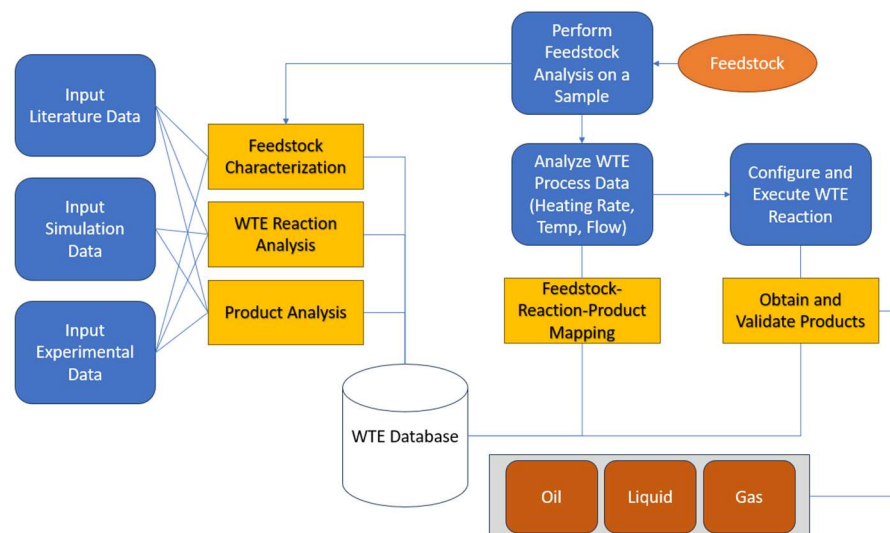


Figure 4. Integrated process model with a WTE database.

2.4. Life Cycle Analysis (LCA)

The primary purpose of this objective was to estimate the sustainability of the products using a cost analysis with an environmental impact assessment. The process was taken from the European ELCD database to conduct the LCA, based on the CML 2001 ecoinvent method, to study 1000 kg of the reactor; if we increased the capacity of the reaction, the emission would increase at the same ratio as the capacity of the reactor.

$$LCC = IC + ESPWF (\text{Cost}_{\text{energy}} + \text{Cost}_{\text{main}})$$

$$LCC = \text{Life Cycle Cost}$$

IC: Initial Cost

ESPWF: Equal Series Present Worth Factors

3. Results and Discussion

3.1. Integration of Thermal Analysis

Thermal analysis was performed to obtain the degradation patterns, temperature profiles, and kinetic analyses to integrate in the process design to optimize conditions for various products. The thermal behavior of the MSW was evaluated at four different heating rates (10, 20, 30, and 40 °C/min). Thermogravimetry (TG-DTG) revealed that mass was continuously lost as the temperature increased. Different stages of mass loss were observed from the TG-DTG curves of the model compounds. During the degradation reaction, dehydration occurred at temperatures below 140 °C, followed by the decomposition of the organic components (Figure 5A). As the material was composed of plastic and paper, therefore, hemicellulose, cellulose, and lignin decomposed at temperatures between 180 °C and 330 °C, 330 °C and 490 °C, and 180 °C and 800 °C, respectively [30].

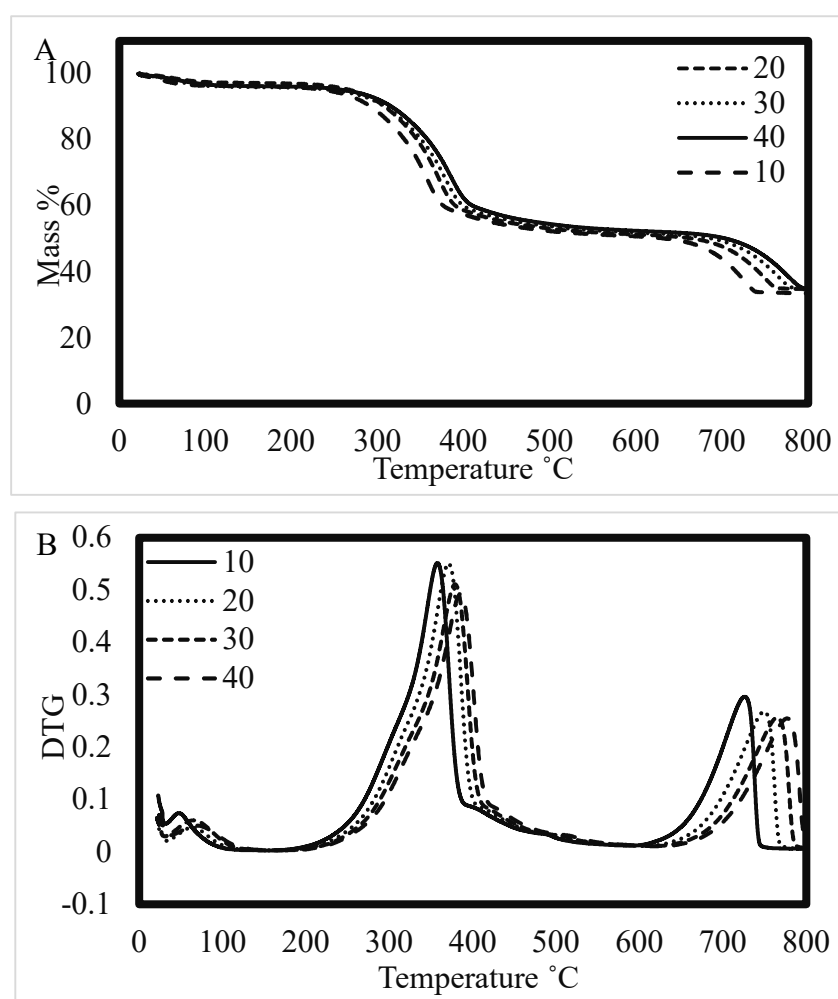


Figure 5. (A) Thermogravimetric curves of the MSW sample at different heating rates. (B) Differential thermogravimetric curves for the MSW sample at four heating rates.

The rate of heating (β) has a substantial impact on the rate of breakdown, total weight loss, and temperature at which the highest weight loss occurs (DTG_{max}). When the heating rate was increased, a higher rate of biomass decomposition was observed, causing the DTG_{max} peaks to move toward the higher temperature region (Figure 5B), which is attributed to the poor conductivity of the biomass. Therefore, a higher heating rate results in a shorter residence time for heat transmission and a higher temperature is needed to

break down organic matter [31]. Interestingly, here, the cellulose breakdown predominated (300–361 °C) with DTG_{max} peaks centered at 273 °C, 276 °C, 279 °C, and 281 °C, at 10 °C/min, 20 °C/min, 30 °C/min, and 40 °C/min, respectively. The weight loss was found to be 18%, 17%, 18%, and 18% at heating rates of 10 °C/min, 20 °C/min, 30 °C/min, and 40 °C/min, respectively. The phenomena of the degradation pattern and temperature associated with each stage are shown in Figure 5A,B. It is obvious that a reaction rate depends primarily on the temperature of the reacting particles, with higher temperatures causing faster reactions with a lower reaction time, thus subsequently increasing the surface temperature. However, MSW almost approaches thermal equilibrium due to lower heating rates and a prolonged thermal energy supply [32]. Thus, the maximum decomposition is shifted to an area of high temperature as a result of a high heating rate. Interestingly, increased gas production is made possible by rapid degradation of volatile elements. Therefore, a lower residue and higher devolatilization rate were obtained [33]. The thermal degradation patterns were also compared with already studied waste samples including plastic [34], plastic waste [35], municipal solid waste [36], solid waste [37], and high-density waste plastic [38], indicating good synchronization which means it can also be used to generate energy products. Furthermore, the pyrolytic decomposition of biomass components occurs individually at a lower heating rate, while the immediate reaction causes the disintegration of various components concurrently at a higher heating rate.

Furthermore, thermal data obtained from TGA experiment were directly stored in the integrated process model for the laboratory-scale reactor for product optimization and control based on the temperature ranges, mass degradation patterns, and heating rates.

3.1.1. Kinetic Analysis

The activation energy (E_a) of the MSW at 10, 20, 30, and 40 °C/min was investigated using the Friedman, FWO, and KAS methods. The process was conducted using slow pyrolysis with gradual, non-isothermal heating. This approach facilitates the determination of kinetic parameters through thermogravimetric analysis, enabling the easy acquisition of temperature-specific data over a prolonged duration. Calculations of the kinetic parameters were made for conversion values ranging from 0.2 to 0.8 and activation energies were calculated using the slopes. For the conversion of 0.1, the regression coefficient is very low; thus, it is considered negligible and therefore ignored [39]. For all models, smooth fits were achieved and for various conversion fractions, the estimated E_a values and R^2 are shown in Table 1. During pyrolysis, it was observed that the E_a values ranged from 132–243 kJ mol⁻¹ when using the OFW technique, 123–227 kJ mol⁻¹ when using the KAS model, and 123–224 kJ mol⁻¹ when using the Starink method. Variation in E_a with conversion values (Figure 6A) indicates that the pyrolysis of the MSW involved a parallel, multi-step devolatilization reaction pathway. The mean E_a values were found to be 185 kJ mol⁻¹, 172 kJ mol⁻¹, and 173 kJ mol⁻¹ by the OFW, KAS, and Starink models, respectively. A comparison of each activation energy at a continuous increase with the conversion point (α) is shown in Figure 6A. The linear plots of the Friedman, OFW, and KAS analyses with small correlation factors suggest the accuracy of the E_a recorded from the experimental data. The kinetic energy values were compared with already studied waste samples including plastic [34], plastic waste [35], municipal solid waste [36], solid waste [37], and high-density waste plastic [38] and indicated correlation, suggesting MSW can also be used effectively to generate energy products. The results obtained from the kinetic model were integrated in a database to optimize the efficiency of the reaction chemistry that was directly linked with the production of biochar, biofuel, and gaseous products.

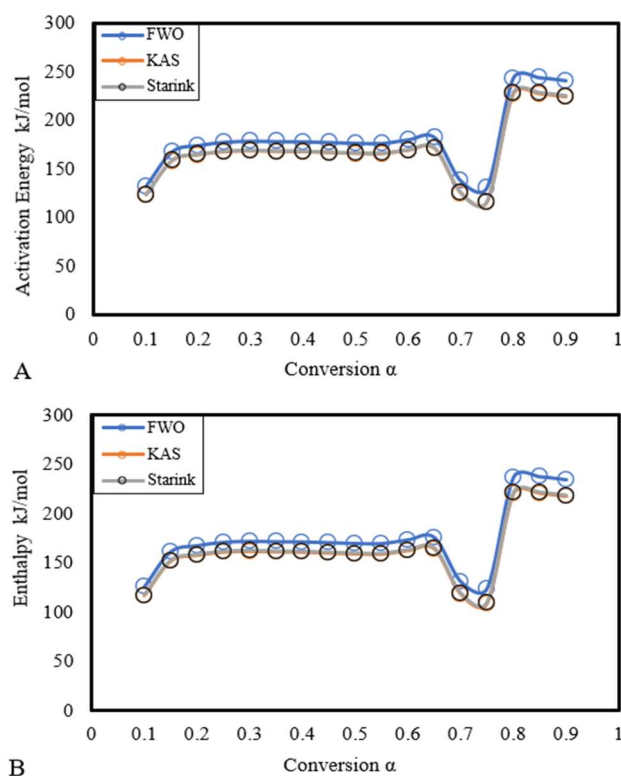


Figure 6. (A) A comparison of each activation energy at a continuous increase with the conversion point (α) for different kinetic models. (B) A comparison of each change in enthalpy (ΔH) at a continuous increase with the conversion point (α) for different kinetic models.

3.1.2. Thermodynamic Analysis

In an inert environment, thermodynamic parameters were determined as shown in Table 1. For designing simulations, reactor thermodynamics parameters play a pivotal role [40]. The average changes in enthalpy (ΔH) were recorded as 178 kJ mol^{-1} , 166 kJ mol^{-1} , and 166 kJ mol^{-1} . A comparison of the ΔH with the conversion point (α) is shown in Figure 6B. A positive ΔH and negative values indicated that MSW undergoes endothermic reactions and exothermic reactions during the pyrolysis process [41]. The reaction mechanism of the MSW comprises a function with multiple reactions because of the complex nature of the material, as shown in Figure 7. However, keeping in view the first and second laws of thermodynamics, the change in the Gibbs' free energy, ΔG , indicates the overall increase in energy of a system and the tendency of a reaction to occur in a particular direction. The results showed increasing trends in the ΔG for the conversion values, 0.2 to 0.8, which confirmed the mechanism's suitability for co-pyrolysis and co-gasification. Significantly, it has been noted that the reaction consistently produced a relatively stable energy output throughout its duration. The results showed decreasing trends in the ΔS for the conversion values, 0.2–0.75, which tend to move a system toward thermodynamic equilibrium by employing physical and chemical processes [42]. This may be attributed to the complex nature of biomass, so properties are difficult to predict.

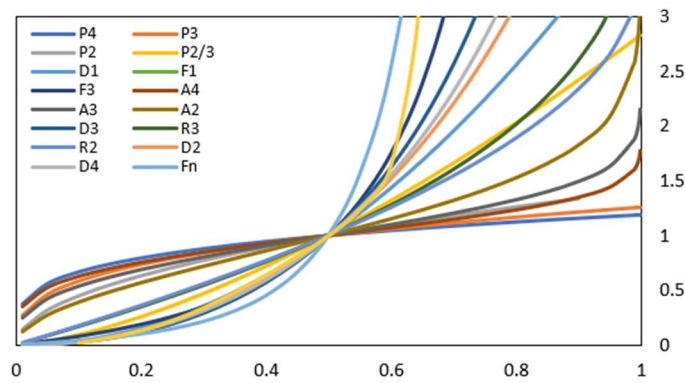


Figure 7. Reaction mechanism of the MSW using reaction kinetics.

Table 1. The thermodynamic parameters with a continuous increase in the conversion (α) with all kinetic models.

Alpha	Activation Energy (E) kJ/mol	Pre-Exponential Factor (A)	R ²	Enthalpy (ΔH) kJ/mol	Gibbs' Free Energy (ΔG) kJ/mol	Entropy (ΔS) J/mol
FWO Model						
0.10	132.37	3.52×10^{97}	0.68	126.02	−1099.63	1606.35
0.15	167.92	2.54×10^{124}	0.91	161.57	−1456.38	2120.52
0.20	174.11	1.20×10^{129}	0.96	167.77	−1518.50	2210.04
0.25	177.56	4.84×10^{131}	0.98	171.21	−1553.09	2259.90
0.30	178.55	2.73×10^{132}	0.99	172.21	−1563.06	2274.27
0.35	178.17	1.40×10^{132}	0.99	171.82	−1559.20	2268.71
0.40	177.97	1.00×10^{132}	1.00	171.63	−1557.27	2265.93
0.45	177.19	2.55×10^{131}	1.00	170.84	−1549.39	2254.56
0.50	176.44	6.93×10^{130}	0.99	170.10	−1541.88	2243.74
0.55	176.26	5.05×10^{130}	0.99	169.91	−1540.05	2241.10
0.60	180.04	3.63×10^{133}	0.98	173.70	−1578.00	2295.80
0.65	182.40	2.20×10^{135}	0.81	176.05	−1601.66	2329.90
0.70	137.77	4.24×10^{101}	0.61	131.42	−1153.84	1684.49
0.75	130.94	2.95×10^{96}	0.55	124.60	−1085.32	1585.73
0.80	243.30	2.25×10^{181}	0.98	236.96	−2212.82	3210.72
0.85	243.87	6.02×10^{181}	0.99	237.52	−2218.49	3218.89
0.90	240.91	3.48×10^{179}	1.00	234.56	−2188.76	3176.04
	185.03			178.69	−1628.09	2367.99
KAS Model						
0.10	123.22	4.33×10^{90}	0.65	116.88	−1007.85	1474.086
0.15	158.35	1.49×10^{117}	0.90	152.00	−1360.35	1982.111
0.20	164.26	4.39×10^{121}	0.95	157.92	−1419.70	2067.653
0.25	167.49	1.21×10^{124}	0.98	161.15	−1452.10	2114.354
0.30	168.30	4.95×10^{124}	0.99	161.96	−1460.24	2126.075
0.35	167.76	1.93×10^{124}	0.99	161.42	−1454.82	2118.263
0.40	167.44	1.11×10^{124}	0.99	161.10	−1451.60	2113.624
0.45	166.55	2.32×10^{123}	1.00	160.20	−1442.59	2100.643
0.50	165.69	5.26×10^{122}	0.99	159.35	−1434.02	2088.298

Table 1. Cont.

Alpha	Activation Energy (E) kJ/mol	Pre-Exponential Factor (A)	R ²	Enthalpy (ΔH) kJ/mol	Gibbs' Free Energy (ΔG) kJ/mol	Entropy (ΔS) J/mol
FWO Model						
0.55	165.40	3.15×10^{122}	0.99	159.05	−1431.07	2084.034
0.60	169.01	1.70×10^{125}	0.98	162.67	−1467.36	2136.338
0.65	170.84	4.09×10^{126}	0.79	164.50	−1485.71	2162.784
0.70	124.87	7.69×10^{91}	0.56	118.53	−1024.44	1498
0.75	115.57	7.19×10^{84}	0.48	109.22	−931.07	1363.429
0.80	227.05	1.18×10^{169}	0.98	220.70	−2049.68	2975.598
0.85	227.27	1.73×10^{169}	0.99	220.92	−2051.91	2978.817
0.90	224.06	6.58×10^{166}	1.00	217.72	−2019.76	2932.471
	172.77			166.43	−1505.07	2190.69
Starink Model						
0.10	123.59	8.19×10^{90}	0.65	117.24	−1011.52	1479.38
0.15	158.73	2.91×10^{117}	0.91	152.39	−1364.19	1987.65
0.20	164.66	8.72×10^{121}	0.96	158.31	−1423.65	2073.35
0.25	167.90	2.43×10^{124}	0.98	161.55	−1456.14	2120.18
0.30	168.71	1.01×10^{125}	0.99	162.37	−1464.35	2132.00
0.35	168.18	3.99×10^{124}	0.99	161.84	−1458.99	2124.28
0.40	167.86	2.30×10^{124}	0.99	161.52	−1455.82	2119.72
0.45	166.97	4.87×10^{123}	1.00	160.63	−1446.86	2106.80
0.50	166.12	1.11×10^{123}	0.99	159.78	−1438.34	2094.52
0.55	165.83	6.71×10^{122}	0.99	159.49	−1435.42	2090.32
0.60	169.45	3.66×10^{125}	0.98	163.11	−1471.78	2142.72
0.65	171.30	9.15×10^{126}	0.79	164.96	−1490.34	2169.47
0.70	125.39	1.89×10^{92}	0.56	119.05	−1029.62	1505.46
0.75	116.18	2.09×10^{85}	0.49	109.84	−937.24	1372.32
0.80	227.70	3.65×10^{169}	0.98	221.35	−2056.21	2985.00
0.85	227.93	5.50×10^{169}	0.99	221.59	−2058.58	2988.42
0.90	224.74	2.12×10^{167}	1.00	218.39	−2026.52	2942.21
	173.26			166.92	−1509.99	2197.78

3.2. Simulation and Comparison of Experimental vs. Model Results

Several product species were discovered through the thermochemical process; the previous results showed that the feasibility of the process is comparable with already studied municipal waste samples. CO concentration is higher as compared to other gaseous products, but if we compare CO₂ with already studied waste samples, it has also been feasible in the gasification experimental data in recent years. CO was higher when compared to PE, PP, and PC at 750 °C but the same when we compared it with waste polythene [43]. When it was compared with H₂, it was lower in PE and PP, as studied by Cao et al. [44], but it was almost comparable to a recent study by Dogu et al. [45]. However, CO₂ percentage was high as compared to polythene bags [46], but lower as compared to Cao et al.'s experimental work related to gasification [44]. Our gasification method used was almost the same when compared to the experimental gasification of general plastic waste [47]. On the basis of these results, it can be predicted the reactor model showed prominent results when compared with experimental data in recent years as shown in Table 2.

Table 2. Comparison of experimental and simulated results.

Feedstock	Gasification	H ₂	CO ₂	CH ₄	CO	C ₂ H ₄	C ₂ H ₆	Reference
Polyethylene (PE)	750 °C	41.67	20.77	30.22	1.14	1.35	4.86	[44]
Polypropylene (PP)	750 °C	36.99	27.82	26.57	1.68	0.86	6.08	[44]
Polycarbonate (PC)	750 °C	36.35	36.80	23.19	2.34	0.27	1.06	[44]
Plastic waste	650–1100 °C	64	4–6	3.30	25.7			[47]
Plastic waste (polyethylene box used for fruit packing)	850–1100 °C	40.86	0.37	9.10	0.1	C ₃ H ₈ (12.8)	28	[46]
Thermoset-insulated wire and cable waste	750 °C (10–14 L in 20 g waste)	4–7		10–13	7–13			[48]
Waste polyethylene	700 °C to 900 °C	16–36	35–20	21–9	20–27	3–4	2	[43]
PE	740 °C (Pyro)	0.8		4.2		11.4	7.3	[45]
PP	760 °C (Pyro)	0.7		4.8		6.6	6.4	[45]
MSW1	750 °C	0.46	3.3	0.03	21.67			Simulation Work
MSW2	750 °C	0.72	3.71	0.06	19.67			Simulation Work
MSW3	750 °C	0.57	4.86	0.03	32.78			Simulation Work
MSW4	750 °C	0.39	3.22	0.05	20.54			Simulation Work
MSW5	750 °C	0.42	4.51	0.02	24.89			Simulation Work

3.3. Integration of Characteristics of Temperature Profiles with Degradation Stages

The mass loss curves provide insights into the physical and chemical transformations that occurred when the MSW was thermally converted into various products [49,50]. Thermogravimetric analysis is commonly employed to quantify the percentage of mass loss in a sample as a function of pyrolysis temperature. In this study, the mass loss percentage of MSW was examined at different heating rates ranging from 5 to 50 °C min⁻¹. Interestingly, the results indicated that the heating rate did not significantly impact the mass loss percentage. The curves displayed a typical pattern of degradation observed in lignocellulosic MSW, which is comparable to the DTG curves obtained from the pyrolysis of various waste materials, including *Delonix regia*, food waste using leachate, potato stalk, and peanut shell [33,51–53].

Based on a literature search, the samples with plastic and paper showed the same trends with the TGA analysis. The mass loss can be classified into three stages, followed by a long tail: the initial stage began at room temperature and extended to a certain temperature, to 110–120 °C for moisture removal, and the second stage occurred with a major degradation pattern to degrade cellulose, hemicellulose, and some lignin components which ranged from 120 °C to 450–520 °C for all observed plastic and paper samples [29,54–62]. The third stage observed when temperature ranged from 520 °C to 800 °C that corresponded to degradation of complex products. Tables 3 and 4 demonstrate the reaction chemistry and activation energy of plastic with temperature profiles that can be used for process optimization.

Table 3. Relationships between the conversion (α), temperature, and activation energy.

Conversion Range (α)	Temperature Range (K)	Reactions	Activation Energy (E_a)
$\alpha \leq 0.17$	25–382	Liberation of retained moisture and volatiles	Increased from starting point to 111–145 kJ mol ⁻¹
$0.17 \leq \alpha \leq 0.5$	382–474	Degradation of secondary and tertiary structured compounds	Increased from 145 to 176 kJ mol ⁻¹ and then decreased from 176 to 131 kJ mol ⁻¹
$0.5 \leq \alpha \leq 0.8$	473–516	Degradation of lignin	Activation Energy from 180 to 220 kJ mol ⁻¹
$0.8 \leq \alpha \leq 1.0$	516–800	Lignin degradation and char formation	Decreased from 240 to 120 kJ mol ⁻¹

Table 4. Relationships between the conversion (α), temperature, and activation energy.

Conversion Range (α)	Temperature Range (K)	Reactions	Activation Energy (E_a)
$\alpha \leq 0.17$	25–365	Liberation of retained moisture	Increased from starting point to 105–143 kJ mol ⁻¹
$0.17 \leq \alpha \leq 0.5$	365–486	Degradation of secondary and tertiary structured compounds	Increased from 135 to 167 kJ mol ⁻¹ and then decreased from slightly with 5 kJ mol ⁻¹
$0.5 \leq \alpha \leq 0.8$	486–511	Degradation of lignin	Increased from 184 to 224 kJ mol ⁻¹
$0.8 \leq \alpha \leq 1.0$	511–800	Lignin degradation and char formation	Decreased from 247 to 112 kJ mol ⁻¹

3.4. Machine Learning Integration

The dataset for machine learning (ML) models including artificial neural networks (ANNs) and advanced regression trees were taken from already built datasets related to plastic pyrolysis. Using ML models, this model accurately predicted biochar outputs from the co-pyrolysis of plastic and paper based on ultimate and proximate analysis results. It was discovered that SANN and C&RT are considered as best models to predict the co-pyrolysis yields. Researchers in the scientific literature who employed machine learning techniques did not compare their outcomes to those of conventional models. Model outcomes provide a way of identifying the influence of characteristics on the prediction of biochar and yields from the co-pyrolysis of biomass and plastics. The data could also assist in forecasting gas outputs from the co-pyrolysis of biomass and plastics.

Figure 8A–D depict the mean values of the features used to train the biochar data, in order to forecast yields using proximate and elemental analysis. For the machine learning analysis, the top six training features proved to have a considerable impact on yield prediction, while other features had a small effect. With mean absolute values of 3.88 and 6.47, respectively, the weight percentage of polymers in the mixture was shown to have a substantial effect on the accuracy of biochar and bio-oil model predictions. This is also evident in the effect of w% P on the prediction: a high value led to a low biochar yield while more plastic in the feedstock led to a higher liquid yield and a lower char yield. Fixed carbon in biomass influences char production; at all pyrolysis temperatures, the presence of more fixed carbon increases char formation. With a mean value of 2.47, the ML analysis indicated that fixed carbon was the second most influential factor in predicting biochar output. A similar conclusion was suggested by the effect of fixed carbon. Co-pyrolysis produced greater solid residue from biomass containing more fixed carbon.

Using machine learning, this work accurately predicted biochar yields from the co-pyrolysis of paper and plastics based on feedstock properties, reaction conditions, and elemental analysis results. It was discovered that dense neural network models excel at predicting biomass and plastics co-pyrolysis yields. The optimization of hyperparameters and the incorporation of proximate analysis into the features enhanced the forecasts for bio-oil substantially. In light of the effects of parameters driving the synthesis of biochar, SHAP analysis helped us comprehend the pyrolysis of the biomass and plastics.

There are some recent studies that have shown that our model is better as compared to already studied ML models. Praporn predicted a model using XBoost to find the synergistic effect of the co-pyrolysis of plastic with a <90% accuracy [63]. Similarly, predicted the biochar percentage using machine learning models with an accuracy of 85% with experimental data [64]. Additionally, a bio-oil predicted model was made with an accuracy of an RMSE of 92% by Tang et al. [65].

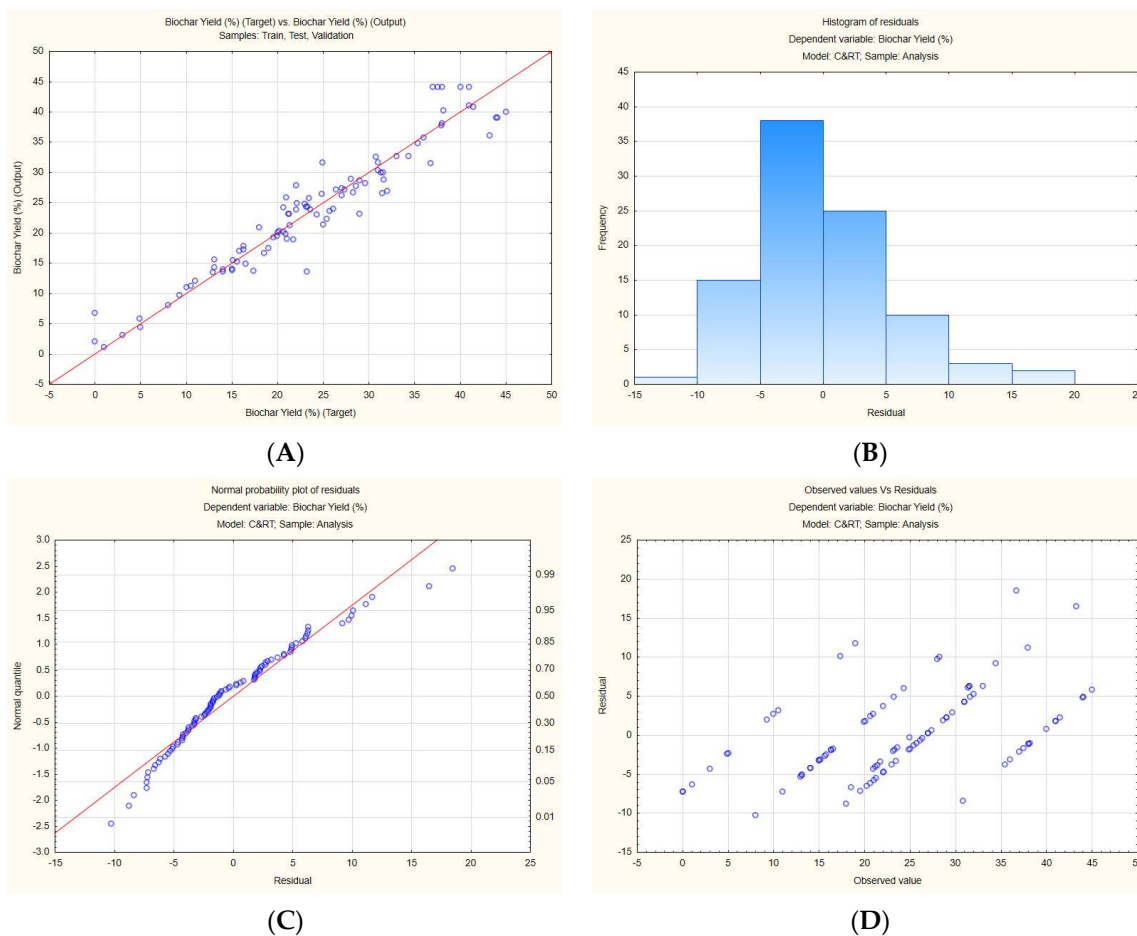


Figure 8. ML models of the biochar yield, a histogram, and a C&RT model (A) target vs output, (B) histogram of residue, (C) normal probability plot and (D) observed vs residuals.

3.5. Life Cycle Analysis

This approach was used to calculate the environmental effects of pyrolyzing mixed plastic waste. However, 1 ton of mixed plastic waste was the functional unit often used in all the impacts discussed below. The net climate change impact is estimated to be 713 kg CO₂ eq./t. Before substitutions, the pyrolysis process accounts for two-thirds of the overall impact, followed by waste collection and sorting at 26% and pyrolysis oil purification at 8%. The 419 kg CO₂ eq./t reduction in total impact can be attributed to the avoidance of naphtha production, which was replaced by pyrolysis oil. This substitution led to a significant decrease in greenhouse gas emissions, thereby contributing to the reduction in the carbon footprint. It is essential to recognize the positive environmental impact of this substitution and give credit to the efforts that led to this achievement. Such efforts could include the development and implementation of sustainable practices that promote the use of alternative fuels or the adoption of cleaner production processes. By acknowledging these contributions, we can encourage further progress toward more sustainable and eco-friendly practices in various industries. Ultimately, this can help to mitigate the adverse effects of climate change and promote a more sustainable future for generations to come.

Energy recovery, though, is a preferable choice for the other aspects considered here. All of the options are depicted by the net savings they bring and the contributions of the material or energy substitutions they bring outweigh their systemic consequences. Chemical recycling and energy recovery have comparable process emissions, but the latter has contributions that are roughly twice as high as the contributions of a naphtha replacement in a pyrolysis system. Apart from a few toxicity impacts (carcinogenic and non-carcinogenic human toxicity as well as terrestrial and freshwater ecotoxicity), a similar pattern is ob-

served for all other impacts measured by the Environmental Footprint techniques. For a 1000 kg reactor, the cost would be CAD 176,093 with a 10-year lifetime warranty, and the profit would be CAD 33,318 based on rough estimation as shown in Table 5. If the process is steady and efficient, it can increase up to CAD 55,000.

Table 5. The product's value with LCC and revenue generation.

	H ₂	CO ₂	CH ₄	CO
Percentage	4	40.5	0.2	240
Value (CAD)	12	3.5	1.2	0.2
Cost	48	141.75	0.24	48
Revenue	CAD 237.99/Run and CAD 33,318/Year			

3.6. Process Controller

By utilizing the three distinctive modes of operation, namely experimental testing, simulation, and literature database analysis, we could effectively establish the critical connections required to pinpoint the ideal product outcomes under precise heating rate and temperature conditions for a given feedstock. This holistic approach to integrated process design not only streamlines the production process but also minimizes operational costs. Instead of allowing reactions to occur at varying temperatures and heating rates, leading to unnecessary time and financial resource wastage, we can strategically control these variables to yield the desired products, as exemplified below.

For every distinct feedstock, the selection of optimal product parameters can be achieved by defining specific operational conditions within a laboratory-scale pyrolysis reactor. This approach empowers us to finetune the pyrolysis process for each unique feedstock, enhancing the efficiency and effectiveness of product development and resource allocation.

Further investigations through a process controller were carried out based on different scenarios of temperature, heating rate, and flow control to evaluate the developed products of the pyrolysis reactions. It was determined that the best heating rate to achieve the highest efficiency occurred at 20 °C/min with a flow rate of 60 mL/min. It was intriguing to observe a significant presence of products associated with them during the experiment. In the reaction, a range of products was formed, including water (H₂O), carbon dioxide (CO₂), carbon monoxide (CO), nitric oxide (NO), and various hydrocarbons such as butane, ethane, ethylene, propylene, acetaldehyde, ammonia (NH₃), and formaldehyde. The order of hydrocarbon evolution was distinct, beginning with acetaldehyde, followed by propylene, ethane, ethylene, butane, and ending with formaldehyde. Oxygenated gases like CO and CO₂ were also observed, with their formation linked to the breakdown of carbon-carbon (C-C) and carbon-oxygen (C-O) bonds. This occurs during the decomposition of hemicellulose and cellulose at temperatures ranging from 240 to 500 °C. The decomposition process extends to lignin and carboxyl (COOH) groups at higher temperatures, leading to the further generation of CO and CO₂. During the initial pyrolysis stage at lower temperatures, there is a predominant release of hydrogen (H₂) and water vapor (H₂O). In contrast, at elevated temperatures during secondary pyrolysis or charring reactions, there is a release of additional H₂, indicating the breakdown of heavier hydrocarbons.

4. Conclusions

The current study provides a well-coordinated process integration for optimizing waste-to-energy processes for municipal solid waste (MSW) that is an essential prerequisite for achieving sustainable technology. The data obtained from thermogravimetric analysis and evolved product analysis were determined by considering different heating rates ranging from 10 to 40 °C min⁻¹ to obtain kinetic and thermodynamic parameters. The results obtained from the characterization through thermogravimetric analysis predicted average values of activation energy of (173–185) kJ/mol and enthalpy of (166–178) kJ/mol

with greater R^2 values that showed the suitability of MSW to generate energy. The product analysis by incorporating coupling between TGA and evolved gas analysis established the potential to obtain useful product species including a high ratio of acetaldehyde >propylene >ethane >ethylene >butane >formaldehyde, which were identified in triplicate at different heating rates. Furthermore, the simulation modeling results showed that the gasification process is also comparable to pyro-gasification, gasification, and catalytic pyrolysis at producing methanol and hydrogen. Several product species have been discovered through the thermochemical process; previous results showed that the feasibility of the process is comparable with already studied municipal waste samples. The experimental and simulation results were compared and gasification occurred at 750 °C. Life cycle analysis and process optimization can bridge the gap for rapid product optimization and profits were estimated at CAD 33,318/Year for a small-scale plant. These values were based on the present value of the products in CAD and can vary with inflation and management practices. All results concluded the suitability of MSW for co-pyrolysis and the co-gasification process with various feedstocks to increase the process efficiency. Hence, we can unlock the potential of waste as a valuable resource for sustainable development. In the case of every unique feedstock, we have the capability to handpick the most suitable product parameters by establishing precise operational conditions within a laboratory-scale pyrolysis reactor. Different stakeholders may benefit from this integrated system including waste management companies, waste treatment plants, pharmaceutical companies using waste problems, and agricultural and farm waste management. This method provides a means to finely calibrate the pyrolysis process to cater to the specific characteristics of every feedstock, ultimately elevating the efficiency and efficacy of our product development efforts and resource utilization. The main contribution is linking products through the co-pyrolysis process by connecting an experimental and simulation setup to obtain optimized products by reducing cost, time, and resources. This might help in the design of a reactor system connected to an experimental and control system where the process can be controlled by changing the temperature, heating rate, and reaction conditions. From the experimental system including, thermogravimetric analysis, evolved product analysis data were generated which were used in kinetic models and reaction chemistry from which an AI system decided the best conditions to perform experiments to obtain different products.

Author Contributions: M.S.A., original writing, methodology, analysis, and validation; H.A.G., editing and review, methodology, validation, supervision, principal investigation, and funding acquisition. All authors have read and agreed to the published version of the manuscript.

Funding: The research was sponsored by Pro-Flange and funded by NSERC 210466, Mitacs 215445, and OCI 202278.

Data Availability Statement: The data presented in this study are available on request from the corresponding author.

Conflicts of Interest: The authors declare no conflicts of interests.

Abbreviations

TGA	Thermogravimetric analyzer
FTIR	Fourier-transform infrared
DTG	Derivative thermogravimetry
Ea	Activation energy
OFW	Ozawa–Flynn–Wall
KAS	Kissinger–Akahira–Sunose
ΔH	Change in enthalpy
ΔS	Change in entropy
ΔG	Change in Gibbs' free energy
A	Pre-exponential factor
R^2	Coefficient of determination

References

1. Fetting, C. *The European Green Deal*; ESDN report; ESDN Office: Vienna, Austria, 2020; p. 53.
2. Commission, E. European Green Deal, Official Website of European Union. Available online: https://commission.europa.eu/strategy-and-policy/priorities-2019-2024/european-green-deal_en (accessed on 20 December 2023).
3. Liu, T.; McConkey, B.; Huffman, T.; Smith, S.; MacGregor, B.; Yemshanov, D.; Kulshreshtha, S. Potential and impacts of renewable energy production from agricultural biomass in Canada. *Appl. Energy* **2014**, *130*, 222–229. [[CrossRef](#)]
4. Antar, M.; Lyu, D.; Nazari, M.; Shah, A.; Zhou, X.; Smith, D.L. Biomass for a sustainable bioeconomy: An overview of world biomass production and utilization. *Renew. Sustain. Energy Rev.* **2021**, *139*, 110691. [[CrossRef](#)]
5. Gourmelon, G. Global plastic production rises, recycling lags. *Vital Signs* **2015**, *22*, 91–95.
6. Shan, C.; Pandyaswargo, A.H.; Onoda, H. Environmental Impact of Plastic Recycling in Terms of Energy Consumption: A Comparison of Japan's Mechanical and Chemical Recycling Technologies. *Energies* **2023**, *16*, 2199. [[CrossRef](#)]
7. Ghiat, I.; Al-Ansari, T. A review of carbon capture and utilisation as a CO₂ abatement opportunity within the EWF nexus. *J. CO₂ Util.* **2021**, *45*, 101432. [[CrossRef](#)]
8. Pant, D.; Misra, S.; Nizami, A.-S.; Rehan, M.; van Leeuwen, R.; Tabacchioni, S.; Goel, R.; Sarma, P.; Bakker, R.; Sharma, N.; et al. Towards the development of a biobased economy in Europe and India. *Crit. Rev. Biotechnol.* **2019**, *39*, 779–799. [[CrossRef](#)] [[PubMed](#)]
9. Williams, J.M.; Bourtsalass, A. Assessment of Co-Gasification Methods for Hydrogen Production from Biomass and Plastic Wastes. *Energies* **2023**, *16*, 7548. [[CrossRef](#)]
10. Grigorescu, A.; Ruiz, V.R.L.; Lincaru, C.; Condrea, E. Specialization Patterns for the Development of Renewable Energy Generation Technologies across Countries. *Energies* **2023**, *16*, 7164. [[CrossRef](#)]
11. Rathour, R.K.; Devi, M.; Dahiya, P.; Sharma, N.; Kaushik, N.; Kumari, D.; Kumar, P.; Baadhe, R.R.; Walia, A.; Bhatt, A.K.; et al. Recent trends, opportunities and challenges in sustainable management of rice straw waste biomass for green biorefinery. *Energies* **2023**, *16*, 1429. [[CrossRef](#)]
12. De Crescenzo, C.; Marzocchella, A.; Karatza, D.; Chianese, S.; Musmarra, D. Autogenerative high-pressure anaerobic digestion modelling of volatile fatty acids: Effect of pressure variation and substrate composition on volumetric mass transfer coefficients, kinetic parameters, and process performance. *Fuel* **2024**, *358*, 130144. [[CrossRef](#)]
13. Siciliano, A.; Limonti, C.; Curcio, G.M. Performance Evaluation of Pressurized Anaerobic Digestion (PDA) of Raw Compost Leachate. *Fermentation* **2021**, *8*, 15. [[CrossRef](#)]
14. Merkle, W.; Baer, K.; Lindner, J.; Zielonka, S.; Ortloff, F.; Graf, F.; Kolb, T.; Jungbluth, T.; Lemmer, A. Influence of pressures up to 50 bar on two-stage anaerobic digestion. *Bioresour. Technol.* **2017**, *232*, 72–78. [[CrossRef](#)]
15. Zhuravel, D.; Samoichuk, K.; Petrychenko, S.; Bondar, A.; Hutsol, T.; Kuboń, M.; Niemiec, M.; Mykhailova, L.; Gródek-Szostak, Z.; Sorokin, D. Modeling of Diesel Engine Fuel Systems Reliability When Operating on Biofuels. *Energies* **2022**, *15*, 1795. [[CrossRef](#)]
16. Ribeiro, L.S.; Stolz, C.M.; Amario, M.; da Silva, A.L.N.; Haddad, A.N. Use of Post-Consumer Plastics in the Production of Wood-Plastic Composites for Building Components: A Systematic Review. *Energies* **2023**, *16*, 6549. [[CrossRef](#)]
17. Alam, M.; Bhavanam, A.; Jana, A.; Viroja, J.K.S.; Peela, N.R. Co-pyrolysis of bamboo sawdust and plastic: Synergistic effects and kinetics. *Renew. Energy* **2020**, *149*, 1133–1145. [[CrossRef](#)]
18. Özsın, G.; Pütün, A.E. A comparative study on co-pyrolysis of lignocellulosic biomass with polyethylene terephthalate, polystyrene, and polyvinyl chloride: Synergistic effects and product characteristics. *J. Clean. Prod.* **2018**, *205*, 1127–1138. [[CrossRef](#)]
19. Wang, X.; Ma, D.; Jin, Q.; Deng, S.; Stančin, H.; Tan, H.; Mikulčić, H. Synergistic effects of biomass and polyurethane co-pyrolysis on the yield, reactivity, and heating value of biochar at high temperatures. *Fuel Process. Technol.* **2019**, *194*, 106127. [[CrossRef](#)]
20. Özsın, G.; Kılıç, M.; Apaydin-Varol, E.; Pütün, A.E.; Pütün, E. A thermo-kinetic study on co-pyrolysis of oil shale and polyethylene terephthalate using TGA/FT-IR. *Korean J. Chem. Eng.* **2020**, *37*, 1888–1898. [[CrossRef](#)]
21. Hu, Q.; Tang, Z.; Yao, D.; Yang, H.; Shao, J.; Chen, H. Thermal behavior, kinetics and gas evolution characteristics for the co-pyrolysis of real-world plastic and tyre wastes. *J. Clean. Prod.* **2020**, *260*, 121102. [[CrossRef](#)]
22. Idris, R.; Chong, C.T.; Asik, J.A.; Ani, F.N. Optimization studies of microwave-induced co-pyrolysis of empty fruit bunches/waste truck tire using response surface methodology. *J. Clean. Prod.* **2020**, *244*, 118649. [[CrossRef](#)]
23. Zhang, J.; Liu, J.; Evrendilek, F.; Zhang, X.; Buyukada, M. TG-FTIR and Py-GC/MS analyses of pyrolysis behaviors and products of cattle manure in CO₂ and N₂ atmospheres: Kinetic, thermodynamic, and machine-learning models. *Energy Convers. Manag.* **2019**, *195*, 346–359. [[CrossRef](#)]
24. Kiminaitė, I.; González-Arias, J.; Striūgas, N.; Eimontas, J.; Seemann, M. Syngas Production from Protective Face Masks through Pyrolysis/Steam Gasification. *Energies* **2023**, *16*, 5417. [[CrossRef](#)]
25. Rotz, S.; Gravely, E.; Mosby, I.; Duncan, E.; Finnis, E.; Horgan, M.; LeBlanc, J.; Martin, R.; Neufeld, H.T.; Nixon, A.; et al. Automated pastures and the digital divide: How agricultural technologies are shaping labour and rural communities. *J. Rural Stud.* **2019**, *68*, 112–122. [[CrossRef](#)]
26. Mabee, W.; Saddler, J. Bioethanol from lignocellulosics: Status and perspectives in Canada. *Bioresour. Technol.* **2010**, *101*, 4806–4813. [[CrossRef](#)] [[PubMed](#)]
27. Darmey, J.; Ahiekpor, J.C.; Narra, S.; Achaw, O.-W.; Ansah, H.F. Municipal Solid Waste Generation Trend and Bioenergy Recovery Potential: A Review. *Energies* **2023**, *16*, 7753. [[CrossRef](#)]

28. Liu, H.; Ahmad, M.S.; Alhumade, H.; Elkamel, A.; Sammak, S.; Shen, B. A hybrid kinetic and optimization approach for biomass pyrolysis: The hybrid scheme of the isoconversional methods, DAEM, and a parallel-reaction mechanism. *Energy Convers. Manag.* **2020**, *208*, 112531. [[CrossRef](#)]
29. Galiwango, E.; Gabbar, H.A. Synergistic interactions, kinetic and thermodynamic analysis of co-pyrolysis of municipal paper and polypropylene waste. *Waste Manag.* **2022**, *146*, 86–93. [[CrossRef](#)]
30. Mumbach, G.D.; Alves, J.L.F.; Da Silva, J.C.G.; De Sena, R.F.; Marangoni, C.; Machado, R.A.F.; Bolzan, A. Thermal investigation of plastic solid waste pyrolysis via the deconvolution technique using the asymmetric double sigmoidal function: Determination of the kinetic triplet, thermodynamic parameters, thermal lifetime and pyrolytic oil composition for clean energy recovery. *Energy Convers. Manag.* **2019**, *200*, 112031. [[CrossRef](#)]
31. Yousef, S.; Eimontas, J.; Striūgas, N.; Zakarauskas, K.; Praspaliauskas, M.; Abdelnaby, M.A. Pyrolysis kinetic behavior and TG-FTIR-GC-MS analysis of metallised food packaging plastics. *Fuel* **2020**, *282*, 118737. [[CrossRef](#)]
32. Badshah, S.L.; Shah, Z.; Alves, J.L.F.; da Silva, J.C.G.; Iqbal, A. Pyrolysis of the freshwater macroalgae *Spirogyra crassa*: Evaluating its bioenergy potential using kinetic triplet and thermodynamic parameters. *Renew. Energy* **2021**, *179*, 1169–1178. [[CrossRef](#)]
33. Periyavaram, S.R.; Uppala, L.; Sivaprakash, S.; Reddy, P.H.P. Thermal behaviour of hydrochar derived from hydrothermal carbonization of food waste using leachate as moisture source: Kinetic and thermodynamic analysis. *Bioresour. Technol.* **2023**, *373*, 128734. [[CrossRef](#)] [[PubMed](#)]
34. Mortezaeikia, V.; Tavakoli, O.; Khodaparasti, M.S. A review on kinetic study approach for pyrolysis of plastic wastes using thermogravimetric analysis. *J. Anal. Appl. Pyrolysis* **2021**, *160*, 105340. [[CrossRef](#)]
35. Al-Moftah, A.M.S.H.; Marsh, R.; Steer, J. Thermal decomposition kinetic study of non-recyclable paper and plastic waste by thermogravimetric analysis. *Chemengineering* **2021**, *5*, 54. [[CrossRef](#)]
36. Wu, L.; Jiang, X.; Lv, G.; Li, X.; Yan, J. Interactive effect of the sorted components of solid recovered fuel manufactured from municipal solid waste by thermogravimetric and kinetic analysis. *Waste Manag.* **2020**, *102*, 270–280. [[CrossRef](#)] [[PubMed](#)]
37. Kuspangaliyeva, B.; Suleimenova, B.; Shah, D.; Sarbassov, Y. Thermogravimetric study of refuse derived fuel produced from municipal solid waste of Kazakhstan. *Appl. Sci.* **2021**, *11*, 1219. [[CrossRef](#)]
38. Yao, Z.; Yu, S.; Su, W.; Wu, W.; Tang, J.; Qi, W. Kinetic studies on the pyrolysis of plastic waste using a combination of model-fitting and model-free methods. *Waste Manag. Res.* **2020**, *38* (Suppl. S1), 77–85. [[CrossRef](#)]
39. Li, J.; Suvarna, M.; Li, L.; Pan, L.; Pérez-Ramírez, J.; Ok, Y.S.; Wang, X. A review of computational modeling techniques for wet waste valorization: Research trends and future perspectives. *J. Clean. Prod.* **2022**, *367*, 133025. [[CrossRef](#)]
40. Shagali, A.A.; Hu, S.; Li, H.; Chi, H.; Qing, H.; Xu, J.; Jiang, L.; Wang, Y.; Su, S.; Xiang, J. Thermal behavior, synergistic effect and thermodynamic parameter evaluations of biomass/plastics co-pyrolysis in a concentrating photothermal TGA. *Fuel* **2023**, *331*, 125724. [[CrossRef](#)]
41. Singh, B.; Singh, S.; Kumar, P. In-depth analyses of kinetics, thermodynamics and solid reaction mechanism for pyrolysis of hazardous petroleum sludge based on isoconversional models for its energy potential. *Process. Saf. Environ. Prot.* **2021**, *146*, 85–94. [[CrossRef](#)]
42. Wen, Y.; Zaini, I.N.; Wang, S.; Mu, W.; Jönsson, P.G.; Yang, W. Synergistic effect of the co-pyrolysis of cardboard and polyethylene: A kinetic and thermodynamic study. *Energy* **2021**, *229*, 120693. [[CrossRef](#)]
43. He, M.; Xiao, B.; Hu, Z.; Liu, S.; Guo, X.; Luo, S. Syngas production from catalytic gasification of waste polyethylene: Influence of temperature on gas yield and composition. *Int. J. Hydrog. Energy* **2009**, *34*, 1342–1348. [[CrossRef](#)]
44. Cao, C.; Bian, C.; Wang, G.; Bai, B.; Xie, Y.; Jin, H. Co-gasification of plastic wastes and soda lignin in supercritical water. *J. Chem. Eng.* **2020**, *388*, 124277. [[CrossRef](#)]
45. Dogu, O.; Pelucchi, M.; Van de Vijver, R.; Van Steenberge, P.H.; D'Hooge, D.R.; Cuoci, A.; Mehl, M.; Frassoldati, A.; Faravelli, T.; Van Geem, K.M. The chemistry of chemical recycling of solid plastic waste via pyrolysis and gasification: State-of-the-art, challenges, and future directions. *Prog. Energy Combust. Sci.* **2021**, *84*, 100901. [[CrossRef](#)]
46. Salavati, S.; Zhang, C.; Zhang, S.; Liu, Q.; Gholizadeh, M.; Hu, X. Cross-interaction during Co-gasification of wood, weed, plastic, tire and carton. *J. Environ. Manag.* **2019**, *250*, 109467. [[CrossRef](#)] [[PubMed](#)]
47. Saebea, D.; Ruengrit, P.; Arpornwichanop, A.; Patcharavorachot, Y. Gasification of plastic waste for synthesis gas production. *Energy Rep.* **2020**, *6*, 202–207. [[CrossRef](#)]
48. Ongen, A. Methane-rich syngas production by gasification of thermoset waste plastics. *Clean Technol. Environ. Policy* **2016**, *18*, 915–924. [[CrossRef](#)]
49. Ceylan, S.; Kazan, D. Pyrolysis kinetics and thermal characteristics of microalgae *Nannochloropsis oculata* and *Tetraselmis* sp. *Bioresour. Technol.* **2015**, *187*, 1–5. [[CrossRef](#)]
50. Maia, A.A.D.; de Morais, L.C. Kinetic parameters of red pepper waste as biomass to solid biofuel. *Bioresour. Technol.* **2016**, *204*, 157–163. [[CrossRef](#)]
51. Nawaz, A.; Kumar, P. A novel pseudo-multicomponent isoconversional approach for the estimation of kinetic and thermodynamic parameters of potato stalk thermal degradation. *Bioresour. Technol.* **2023**, *376*, 128846. [[CrossRef](#)]
52. Rammohan, D.; Kishore, N.; Uppaluri, R. Insights on kinetic triplets and thermodynamic analysis of *Delonix regia* biomass pyrolysis. *Bioresour. Technol.* **2022**, *358*, 127375. [[CrossRef](#)]
53. Kushwaha, R.; Singh, R.S.; Mohan, D. Comparative study for sorption of arsenic on peanut shell biochar and modified peanut shell biochar. *Bioresour. Technol.* **2023**, *375*, 128831. [[CrossRef](#)] [[PubMed](#)]

54. Lin, K.; Tian, L.; Zhao, Y.; Zhao, C.; Zhang, M.; Zhou, T. Pyrolytic characteristics of fine materials from municipal solid waste using TG-FTIR, Py-GC/MS, and deep learning approach: Kinetics, thermodynamics, and gaseous products distribution. *Chemosphere* **2022**, *293*, 133533. [[CrossRef](#)] [[PubMed](#)]
55. Xu, M.; Cao, C.; Hu, H.; Ren, Y.; Guo, G.; Gong, L.; Zhang, J.; Zhang, T.; Yao, H. Perspective on the disposal of PVC artificial leather via pyrolysis: Thermodynamics, kinetics, synergistic effects and reaction mechanism. *Fuel* **2022**, *327*, 125082. [[CrossRef](#)]
56. Liu, H.; Wang, C.; Zhang, J.; Zhao, W.; Fan, M. Pyrolysis Kinetics and Thermodynamics of Typical Plastic Waste. *Energy Fuels* **2020**, *34*, 2385–2390. [[CrossRef](#)]
57. Zaker, A.; Chen, Z.; Zaheer-Uddin, M.; Guo, J. Co-pyrolysis of sewage sludge and low-density polyethylene—A thermogravimetric study of thermo-kinetics and thermodynamic parameters. *J. Environ. Chem. Eng.* **2021**, *9*, 104554. [[CrossRef](#)]
58. Xu, F.; Wang, B.; Yang, D.; Ming, X.; Jiang, Y.; Hao, J.; Qiao, Y.; Tian, Y. TG-FTIR and Py-GC/MS study on pyrolysis mechanism and products distribution of waste bicycle tire. *Energy Convers. Manag.* **2018**, *175*, 288–297. [[CrossRef](#)]
59. Sun, H.; Bi, H.; Jiang, C.; Ni, Z.; Tian, J.; Zhou, W.; Qiu, Z.; Lin, Q. Experimental study of the co-pyrolysis of sewage sludge and wet waste via TG-FTIR-GC and artificial neural network model: Synergistic effect, pyrolysis kinetics and gas products. *Renew. Energy* **2022**, *184*, 1–14. [[CrossRef](#)]
60. Fang, S.; Lin, Y.; Huang, Z.; Huang, H.; Chen, S.; Ding, L. Investigation of co-pyrolysis characteristics and kinetics of municipal solid waste and paper sludge through TG-FTIR and DAEM. *Thermochim. Acta* **2021**, *700*, 178889. [[CrossRef](#)]
61. Kremer, I.; Tomić, T.; Katančić, Z.; Erceg, M.; Papuga, S.; Vuković, J.P.; Schneider, D.R. Catalytic pyrolysis of mechanically non-recyclable waste plastics mixture: Kinetics and pyrolysis in laboratory-scale reactor. *J. Environ. Manag.* **2021**, *296*, 113145. [[CrossRef](#)]
62. Zhang, Y.; Ahmad, M.S.; Shen, B.; Yuan, P.; Shah, I.A.; Zhu, Q.; Ibrahim, M.; Bokhari, A.; Klemeš, J.J.; Elkamel, A. Co-pyrolysis of lychee and plastic waste as a source of bioenergy through kinetic study and thermodynamic analysis. *Energy* **2022**, *256*, 124678. [[CrossRef](#)]
63. Prasertpong, P.; Onsree, T.; Khuenkaeo, N.; Tippayawong, N.; Lauterbach, J. Exposing and understanding synergistic effects in co-pyrolysis of biomass and plastic waste via machine learning. *Bioresour. Technol.* **2023**, *369*, 128419. [[CrossRef](#)] [[PubMed](#)]
64. Chen, M.-W.; Chang, M.-S.; Mao, Y.; Hu, S.; Kung, C.-C. Machine learning in the evaluation and prediction models of biochar application: A review. *Sci. Prog.* **2023**, *106*, 00368504221148842. [[CrossRef](#)] [[PubMed](#)]
65. Tang, Q.; Chen, Y.; Yang, H.; Liu, M.; Xiao, H.; Wu, Z.; Chen, H.; Naqvi, S.R. Prediction of Bio-oil Yield and Hydrogen Contents Based on Machine Learning Method: Effect of Biomass Compositions and Pyrolysis Conditions. *Energy Fuels* **2020**, *34*, 11050–11060. [[CrossRef](#)]

Disclaimer/Publisher’s Note: The statements, opinions and data contained in all publications are solely those of the individual author(s) and contributor(s) and not of MDPI and/or the editor(s). MDPI and/or the editor(s) disclaim responsibility for any injury to people or property resulting from any ideas, methods, instructions or products referred to in the content.